J. Fluid Mech. (2018), *vol.* 851, *pp.* 391–415.
doi:10.1017/jfm.2018.508

Fully resolved measurements of turbulent boundary layer flows up to $Re_\tau = 20\,000$

M. Samie[1,†], I. Marusic[1], N. Hutchins[1], M. K. Fu[2], Y. Fan[2], M. Hultmark[2] and A. J. Smits[2]

[1]Department of Mechanical Engineering, University of Melbourne, Victoria 3010, Australia

[2]Department of Mechanical and Aerospace Engineering, Princeton University, Princeton, NJ 08544, USA

(Received 1 January 2018; revised 2 May 2018; accepted 19 June 2018;
first published online 20 July 2018)

Fully resolved measurements of turbulent boundary layers are reported for the Reynolds number range $Re_\tau = 6000$–$20\,000$. Despite several decades of research in wall-bounded turbulence there is still controversy over the behaviour of streamwise turbulence intensities near the wall, especially at high Reynolds numbers. Much of it stems from the uncertainty in measurement due to finite spatial resolution. Conventional hot-wire anemometry is limited for high Reynolds number measurements due to limited spatial resolution issues that cause attenuation in the streamwise turbulence intensity profile near the wall. To address this issue we use the nano-scale thermal anemometry probe (NSTAP), developed at Princeton University to conduct velocity measurements in the high Reynolds number boundary layer facility at the University of Melbourne. The NSTAP has a sensing length almost one order of magnitude smaller than conventional hot-wires. This enables us to acquire fully resolved velocity measurements of turbulent boundary layers up to $Re_\tau = 20\,000$. Results show that in the near-wall region, the viscous-scaled streamwise turbulence intensity grows with Re_τ in the Reynolds number range of the experiments. A second outer peak in the streamwise turbulence intensity is also shown to emerge at the highest Reynolds numbers. Moreover, the energy spectra in the near-wall region show excellent inner scaling over the small to moderate wavelength range, followed by a large-scale influence that increases with Reynolds number. Outer scaling in the outer region is found to collapse the energy spectra over high wavelengths across various Reynolds numbers.

Key words: turbulent boundary layers, turbulent flows

1. Introduction

Wall-bounded turbulent flows are ubiquitous in nature and technological applications. In many of these applications the Reynolds number is high, namely of the order of 10^5–10^7, which is out of reach for direct numerical simulations (DNS). An alternative approach, which is not as computationally demanding as DNS, yet captures much of the three-dimensional motions in a turbulent flow, is large eddy simulation (LES). However, the only economical way to perform high Reynolds number LES in the

† Email address for correspondence: msamie@student.unimelb.edu.au

presence of the wall is to compute the outer layer and empirically model the inner layer using wall models (Piomelli & Balaras 2002). This calls for reliable measurements very close to the wall at high Reynolds number to improve our understanding of the underlying physics of these fluid flows.

Several decades of research in wall-bounded turbulence has proved that acquiring unambiguous high-Re experimental data, especially close to the wall, is challenging. That is partially due to the fact that the size of the smallest-scale motions, which are predominant near the wall, decreases with the increase in Reynolds number. This leads to uncertainty in measurement of turbulence intensities very close to the wall as a result of finite spatial resolution of various experimental techniques. Friction Reynolds number in wall-bounded turbulence is defined as the ratio of the largest to the smallest scales, $Re_\tau = \delta/(\nu/u_\tau)$ (where δ is the boundary layer thickness, ν is the kinematic viscosity and u_τ is the friction velocity). In the laboratory, one way to achieve high Reynolds number is through decreasing the size of the smallest scales ($\sim\nu/u_\tau$) and using very small sensors for the measurements. This approach has been followed in the Princeton Superpipe and High Reynolds Number Testing Facility (HRTF), where as a result, the conventional hot-wires are excessively large to resolve the smallest-scale motions at the highest Reynolds numbers. A nano-scale thermal anemometry probe (NSTAP) was developed by Bailey *et al.* (2010) to overcome this problem, and has been widely used for high-Re measurements in pipe and boundary layer flows ever since (Hultmark *et al.* 2012, 2013; Rosenberg *et al.* 2013; Vallikivi, Ganapathisubramani & Smits 2015*a*; Vallikivi, Hultmark & Smits 2015*b*). An alternative approach to increase Re is to increase the size of the largest scales ($\sim\delta$), which necessitates construction of very large wind tunnels such as the large University of Melbourne wind tunnel (Nickels *et al.* 2005), the Flow Physics Facility at the University of New Hampshire (Vincenti *et al.* 2013) and the CICLoPE facility at the University of Bologna (Talamelli *et al.* 2009). In spite of following the above-mentioned approaches, the spatial resolution issue has remained unavoidable at the highest Reynolds numbers. For example, the viscous-scaled sensor length, $l^+ = lu_\tau/\nu$, for NSTAP at $Re_\tau > 68\,000$ in the Superpipe is greater than 30 (where l is the sensor length), and the conventional hot-wire's viscous-scaled length is greater than 20 for the highest Re_τ achievable in the mentioned large wind tunnels, leading to significant attenuation of energy in the near-wall region (Hutchins *et al.* 2009; Vincenti *et al.* 2013; Örlü *et al.* 2017).

As a result of spatial resolution limitations in high-Re turbulence measurements, the near-wall scaling of turbulence intensities, especially the streamwise turbulence intensity $\overline{u^2}$, is still under discussion. The distribution of $\overline{u^{2+}} = \overline{u^2}/u_\tau^2$ shows a distinct peak referred to as the 'inner peak', $\overline{u^{2+}}_{max}$, in the near-wall region at the inner normalised wall distance $z^+ = zu_\tau/\nu \approx 15$. Lee & Moser (2015) compiled results from several DNS studies in turbulent pipe, channel and boundary layer flows showing an increasing trend with Re_τ for $\overline{u^{2+}}_{max}$ with a log–linear relation in the Reynolds number range $Re_\tau = 1000$–5200. Review of the experimental studies, on the other hand, is less conclusive mainly because of spatial resolution issues. While most of the studies show that $\overline{u^{2+}}_{max}$ exhibits a weak Re dependence (Klewicki & Falco 1990; De Graaff & Eaton 2000; Metzger *et al.* 2001; Hutchins & Marusic 2007; Willert *et al.* 2017), some researchers have reported that it is invariant with Re (Fernholz & Finley 1996; Mochizuki & Nieuwstadt 1996; Hultmark *et al.* 2012, 2013; Vallikivi *et al.* 2015*b*).

Apart from the inner peak, a second outer peak in $\overline{u^{2+}}$ has been reported for very high Reynolds number turbulent wall-bounded flows (e.g. Morrison *et al.* 2004;

Metzger, McKeon & Holmes 2007; Hultmark *et al.* 2012; Vallikivi *et al.* 2015*b*; Willert *et al.* 2017). However, the presence of this peak and as to whether it is a peak or a plateau is still unclear since spatial resolution in many of these studies degrades at the very high-*Re* measurements. According to Hutchins *et al.* (2009) the spatial resolution filtering extends to wall distances higher than the immediate near-wall region and may produce an artificial outer peak by attenuating the turbulence intensity profile in the near-wall region while leaving the log layer virtually unaffected (see figure 5 in Hutchins *et al.* (2009)). The prediction of a second outer peak arising at high Reynolds number would be notable as it may indicate the presence of new outer phenomena (Marusic *et al.* 2010*b*; Hultmark *et al.* 2012).

In an attempt to attain fully resolved measurements we combine both approaches previously followed to avoid spatial resolution problems. The NSTAP is employed to conduct velocity measurements in the large University of Melbourne wind tunnel. The measurements cover a friction Reynolds number range $Re_\tau = 6000$–$20\,000$ and the viscous-scaled sensor length is in the range $l^+ = 2.5$–3.5, which is unique for these high values of Reynolds number. This allows us to compare the current results with the DNS data close to the wall and reveal that the inner peak in $\overline{u^{2+}}$ (for turbulent boundary layers up to $Re_\tau = 20\,000$) closely follows the increasing trend previously reported by Lee & Moser (2015) from DNS results. Moreover, comparison of the pre-multiplied energy spectra from fully resolved measurements and DNS in the Reynolds number range 500–20 000 at $z^+ \approx 15$ shows that the inner scaling collapses the spectra over the very small to moderate wavelength range, followed by a large-scale influence that grows with Reynolds number.

2. Experimental methods

2.1. *Flow facility*

Experiments were conducted in the high Reynolds number boundary layer wind tunnel located at the University of Melbourne. This tunnel has a working section of nominally 27 m × 2 m × 1 m. Upstream flow is carefully conditioned before passing through a three-dimensional contraction with an area reduction ratio of 6.2. The free-stream turbulence intensity ($\sqrt{\overline{u^2}}/U_\infty$) is less than 0.05 % at the start of the working section and in the range of 0.15–0.2 % at $x = 22$ m from the start of the working section for the free-stream flow range of 10–40 m s^{-1}. Measurements were made on the tunnel floor at varying streamwise locations between 6 and 22 m downstream of the tripped inlet at free-stream velocities $U_\infty = 20$ and 30 m s^{-1}. The flow is tripped at the entrance to the working section by a 35 mm wide stripe of P40 grit sand paper (with a grit size of 425–500 μm) to produce a canonical boundary layer. As the working section is operated above atmospheric pressure a zero pressure gradient is maintained by bleeding the top wall boundary layer, resulting in a constant free-stream mean velocity along the entire working section maintained to within ±0.5 %.

The anemometry probe is positioned with respect to the wall before commencing a measurement using a depth measuring displacement microscope from Titan Tool Supply with a positioning accuracy of ±1 μm. A stepper motor traverse with a RENISHAW RGH24-type linear optical encoder was used to position the probe. Positional accuracy of the encoder is ±0.5 μm and that of the traverse is ±5 μm. Further details of the facility are given by Marusic *et al.* (2015).

2.2. *Probes*

Nano-scale thermal anemometry probes (NSTAPs) manufactured at Princeton University with the sensing element length of 60 μm along with a standard boundary layer hot-wire probe were employed for the measurement of velocity fluctuations. Design and fabrication of the NSTAP are described by Vallikivi & Smits (2014). The viscous-scaled sensor length l^+ was between 2.4 and 3.5 for the NSTAP for various Reynolds numbers ranging $Re_\tau = 6000$–$20\,000$. Therefore, the small-scale motions are fully resolved in all the NSTAP measurements (Chin *et al.* 2009). Standard hot-wires were also used for comparison, consisting of slightly modified Dantec 55P15 single-normal boundary layer type probes with prong tip spacing of 1.5 mm. Wollaston wires were soldered to the prong tips and etched to reveal a 2.5 μm diameter, 0.5 mm long platinum sensing element in the middle, leading to a length-to-diameter ratio of 200 to minimise end-conduction effect (Ligrani & Bradshaw 1987; Hutchins *et al.* 2009); l^+ for the standard hot-wires is between 20 and 29.

2.3. *Constant temperature anemometry*

Anemometry probes are operated with two constant temperature anemometers throughout the measurements. An in-house Melbourne University constant temperature anemometer (MUCTA) was used to operate the standard hot-wires with an overheat ratio of 1.8. The NSTAP was operated using a Dantec Streamline constant temperature anemometer system in the 1 : 1 bridge mode with an external resistor and the overheat ratio set to 1.6. The system responses of both MUCTA and Dantec anemometers were verified using a square-wave electronic test to ensure a second-order response. A frequency response (based on the −3 dB cutoff) was between 15 and 30 kHz for the standard hot-wires operated with the MUCTA, and between 150 and 200 kHz for the NSTAP operated with the Dantec system in quiescent air.

Hot-wire signals were sampled using an analogue to digital converter (DT9836 from Data Translation) with a resolution of 16 bits in the range of ±10 V. The sampling frequency was set to $f_s = 50$ kHz for the free-stream velocity $U_\infty = 20$ m s^{-1} and $f_s = 80$ kHz for $U_\infty = 30$ m s^{-1}. In order to avoid aliasing in the sampled signals, they were low-pass filtered using an 8-pole Butterworth filter from Frequency Devices, Inc. model 9002 at $f_c = f_s/2$ before sampling. This leads to a viscous-scaled filtering frequency in the range of $0.85 < f_c^+ = f_c\nu/u_\tau^2 < 0.99$ for $U_\infty = 20$ m s^{-1} and $f_c^+ \approx 0.74$ for $U_\infty = 30$ m s^{-1}. Therefore, it was ensured that the entire energetic frequencies were resolved for all the measurements, following Hutchins *et al.* (2009) who showed that the energy content beyond $f_{max}^+ \approx 1/3$ is negligible across various Reynolds numbers. The total sampling time at each wall-normal location z is given by T and is outer normalised to give the boundary layer turnovers TU_∞/δ. In order to obtain converged statistics and partially converged spectra, this number should be large to capture several hundreds of the largest structures past the probe. In the present study $TU_\infty/\delta = 12\,000$–$15\,000$ for all measurements.

Calibration of the anemometry probes was performed statically inside the tunnel in the free stream against a Pitot-static tube before and after each full traverse. Fourth-order polynomial curves were fitted to the calibration data. In order to account for the calibration drift, the anemometry probe was periodically traversed to the free stream (every sixth measurement point), during the boundary layer profile measurement, and sampled against the Pitot-static tube to obtain calibration points at the profile measurement speed. This procedure provides a time record of the

Re_τ	x (m)	U_∞ (m s^{-1})	ν/u_τ (μm)	u_τ (m s^{-1})	TU_∞/δ	Δt^+	l^+	l/η_{min}	Probes	N	Symbols/ lines
6000	6.3	20	23.6	0.69	14 400	0.58	21	9.9	HW	—	——
							2.5	1.2	NSTAP (avg.)	4	—
10 000	13	20	24.4	0.66	12 500	0.54	21	9.9	HW	—	——
							2.5	1.2	NSTAP (avg.)	4	—
14 500	21	20	25.2	0.65	14 000	0.51	20	9.4	HW	—	——
							2.4	1.1	NSTAP (avg.)	3	—
20 000	21	30	17.2	0.93	12 500	0.68	29	14	HW	—	——
							3.5	1.6	NSTAP (avg.)	5	—

TABLE 1. Summary of the experimental conditions.

probe's drift during the profile measurement, which can later be extrapolated to all calibration speeds to obtain the modified calibration curve at each speed. This procedure is described in detail by Talluru *et al.* (2014). Drift for the current NSTAP measurements was always less than 0.5 % between consecutive periodic free-stream checks and less than 2 % between the pre- and post-calibrations. Moreover, the drift for the 2.5 μm diameter hot-wire measurements was always less than 1 % between pre- and post-calibration. The temperature was measured continuously in the undisturbed free stream for the entire duration of the experiment using a DP25 series thermocouple from Omega, USA with a resolution of 0.1 °C. The temperature variation throughout the measurements was within ±1.5 °C for the measurements conducted at the nominal velocity of 20 m s^{-1} and ±3 °C for those conducted at the nominal velocity of 30 m s^{-1}. The correction scheme for temperature variations proposed by Hultmark & Smits (2010) was employed and no significant change in the results was observed with and without applying the temperature correction scheme.

2.4. *Experimental conditions*

Table 1 summarises the experimental conditions of all the measurements. Wall-normal traverses were made at three streamwise locations downstream of the tripped inlet given by x. U_∞ is the free-stream velocity and u_τ is the friction velocity. The measured mean velocity U is fitted to the composite profile of Chauhan, Monkewitz & Nagib (2009) by a least-squares procedure (with log-law constants $\kappa = 0.384$ and $B = 4.17$) to determine u_τ and δ, where δ is the boundary layer thickness, which is inherently larger than δ_{99}. R-squared values were not smaller than 0.9997 for the curve fits in various cases. Chauhan *et al.* (2009) have shown that the u_τ values obtained by this method are within ±2 % of those determined by direct oil-film interferometry measurements. We compared the estimated u_τ with that directly measured with a floating element at $x = 21$ m at $U_\infty = 20$ m s^{-1} in this facility by Baars *et al.* (2016) and observed an agreement to within ±1 %. Baars *et al.* (2016) also verified the value of κ in this facility independently by comparing the floating element data with the Coles–Fernhols relation of the form $U^+_\infty = 1/\kappa\ \ln(Re_\theta) + C$. The probe length is shown in table 1 in viscous scaling (l^+) and in terms of the smallest measured Kolmogorov length scale (l/η_{min}) at each Reynolds number. The friction Reynolds number $Re_\tau = u_\tau\delta/\nu$ is calculated using the fitted composite profile. Multiple measurement repeats were carried out at each Reynolds number with different NSTAP

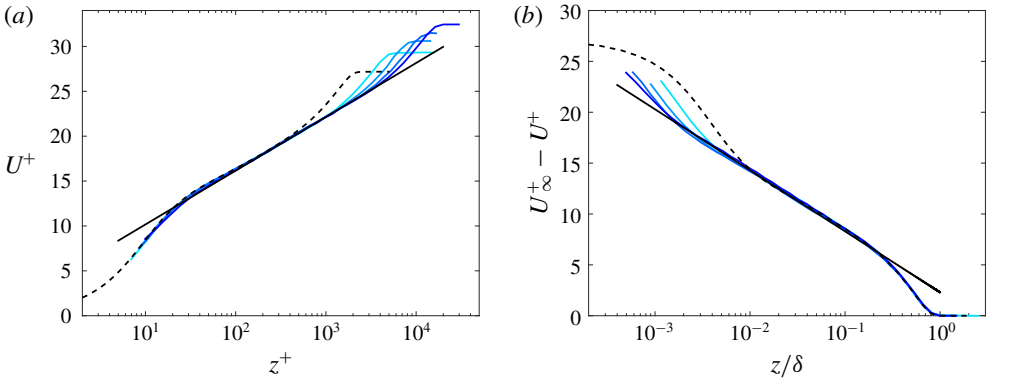

FIGURE 1. (Colour online) (*a*) Inner normalised mean velocity U^+ against inner normalised wall distance z^+. The straight line indicates the log law $U^+ = 1/0.384 \ln(z^+) + 4.17$. (*b*) Velocity defect law against outer normalised wall distance z/δ. The straight line corresponds to the relation $U^+ = 2.3 - 1/0.384 \ln(z/\delta)$. ——, NSTAP, $Re_\tau = 6000$; ——, NSTAP, $Re_\tau = 10\,000$; ——, NSTAP, $Re_\tau = 14\,500$; ——, NSTAP, $Re_\tau = 20\,000$; - - - -, DNS of turbulent boundary layer at $Re_\tau = 2500$ from Sillero, Jiménez & Moser (2013).

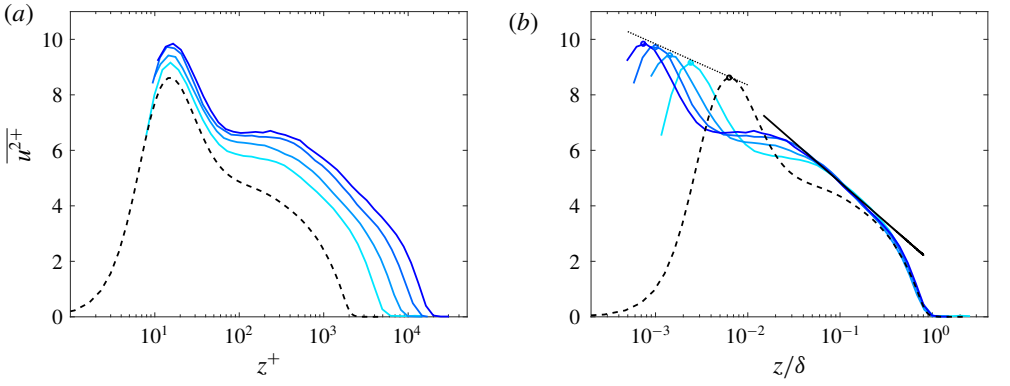

FIGURE 2. (Colour online) Inner normalised turbulence intensity profile $\overline{u^{2+}}$ against (*a*) inner normalised wall distance z^+ and (*b*) outer normalised wall distance z/δ. The dotted line corresponds to $\overline{u^{2+}}_{max} = 5.4 - 0.642 \log(z_{max}/\delta)$ and the straight line indicates $\overline{u^{2+}} = 1.95 - 1.26 \log(z/\delta)$. Other lines are the same as in figure 1.

probes (the number of these repeats is given by N in table 1) and one measurement with the standard hot-wire. Validation of the NSTAP and selection of reliable NSTAPs have been achieved through the procedure detailed in appendix A. Repeats of the reliable NSTAPs are averaged to obtain the averaged NSTAP statistics and energy spectra at each Re_τ.

3. Results and discussion

3.1. *Mean flow and streamwise turbulence intensity*

Figures 1(*a*) and 1(*b*) show the mean velocity profiles as measured by the NSTAP together with the DNS of boundary layer data from Sillero *et al.* (2013) at $Re_\tau \approx 2500$

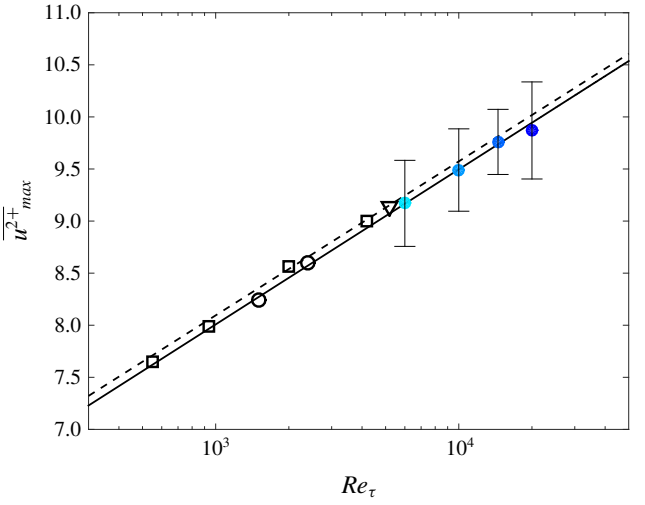

FIGURE 3. (Colour online) Dependence of maximum of $\overline{u^{2+}}$ on Re_τ. ●, NSTAP; ○, DNS of turbulent boundary layer from Sillero *et al.* (2013); □, DNS of channel flow from Lozano-Durán & Jiménez (2014); ▽, DNS of channel flow from Lee & Moser (2015); ——, $\overline{u^{2+}}_{max} = 3.54 + 0.646\log(Re_\tau)$; - - - -, $\overline{u^{2+}}_{max} = 3.66 + 0.642\log(Re_\tau)$ from Lee & Moser (2015).

in inner normalised and velocity defect form, respectively. Figures 2(*a*) and 2(*b*) show the turbulence intensity profiles scaled with u_τ at various Re_τ against viscous and outer normalised wall distance, respectively. A good outer-scaling collapse is observed for nominally $z/\delta \geqslant 0.2$ in the Reynolds number range $Re_\tau = 2500$–$20\,000$. In the overlap region one observes that the streamwise turbulence intensity profiles follow the logarithmic relation

$$\overline{u^{2+}} = B_1 - A_1\log(z/\delta), \tag{3.1}$$

with $A_1 = 1.26$ and $B_1 = 1.95$ for $6000 \leqslant Re_\tau \leqslant 20\,000$. This logarithmic behaviour of the streamwise turbulence intensity has been previously demonstrated by Hultmark *et al.* (2012), Marusic *et al.* (2015) and Vallikivi *et al.* (2015*b*), among others. NSTAP measurements exhibit a clear growth of the inner peak in the streamwise turbulence intensity, $\overline{u^{2+}}_{max}$, located at $z^+ \approx 15$ with increasing Re_τ. As $l^+ < 3.5$ (i.e. the near-wall region is fully resolved) for all the NSTAP measurements, we can compare the trend in $\overline{u^{2+}}_{max}$ from our results with that from the DNS results at lower Reynolds numbers. The inner peak values scaled on u_τ are plotted against Re_τ in figure 3 for the data from the current study as well as those from various DNS studies. Error bars correspond to 95 % confidence interval calculated for the finite number of experiment repeats N at each Re_τ assuming a t distribution for the experiment repeats (Coleman & Steele 2009). It is evident that our experimental results extend the log–linear trend of $\overline{u^{2+}}_{max}$ previously reported for the DNS data by Lee & Moser (2015) and Lozano-Durán & Jiménez (2014). Dependence of the peak of $\overline{u^{2+}}$ on Re_τ was fitted to the boundary layer DNS and our higher Re data to obtain

$$\overline{u^{2+}}_{max} = 3.54 + 0.646\log(Re_\tau). \tag{3.2}$$

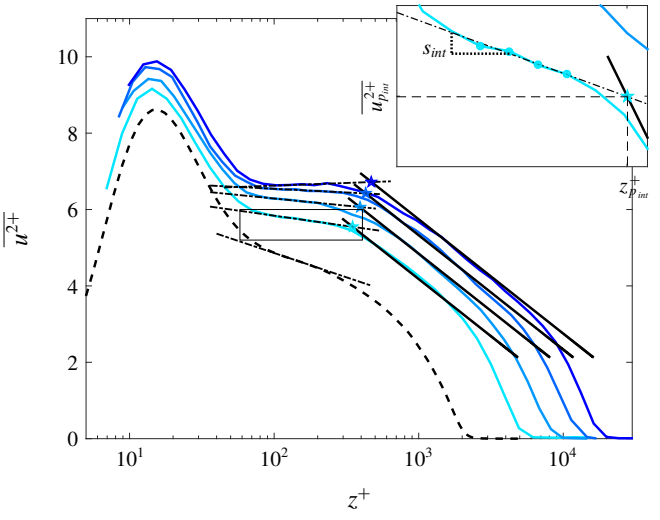

FIGURE 4. (Colour online) Upper bound for the outer peak of streamwise turbulence intensity indicated by the pentagrams for various Reynolds numbers. The inset shows the zoomed view of the region bounded by the rectangle demonstrating the slope (S_{int}) and x ($z^+_{p\ int}$) and y ($\overline{u^{2+}_{p\ int}}$) coordinates of the intersection of the tangent line (to the intermediate region) with the logarithmic relation for $Re_\tau = 6000$. Straight solid lines correspond to (3.1) for $Re_\tau = 6000$, 10 000, 14 500 and 20 000; straight dot-dashed lines indicate the logarithmic tangent lines to the intermediate region ($100 \leqslant z^+ \leqslant 3.9Re_\tau^{1/2}$) of turbulence intensity profiles. Other lines are as in figure 1.

This relation is shown in figure 3 together with the relation $\overline{u^{2+}}_{max} = 3.66 + 0.646\log(Re_\tau)$ proposed by Lee & Moser (2015). One can see that the agreement between (3.2) and the fit by Lee & Moser (2015) is within the measurement uncertainty.

Now we address the controversies regarding the outer peak in $\overline{u^{2+}}$. One can see that locating the outer peak accurately is challenging due to the lack of smoothness of the intensity profiles in the experimental results, and certainly, only the highest Reynolds number case shown in figure 2 shows any possible sign of an outer peak. This issue can be remedied by attempting to find an upper bound for the outer peak instead of the peak itself by drawing a tangent line to the inflection point in the intermediate region of $\overline{u^{2+}}$ (located in the viscous scaled wall-normal range $100 \leqslant z^+ \leqslant 3.9Re_\tau^{1/2}$), and intersecting it with the logarithmic relation as shown in figure 4. To this end, we first need to find the inflection point in the intermediate region of $\overline{u^{2+}}$. The inflection point is associated with the point where $\mathrm{d}^2(\overline{u^{2+}})/\mathrm{d}(\log(z^+))^2$ crosses zero and also $\mathrm{d}(\overline{u^{2+}})/\mathrm{d}(\log(z^+))$ adopts its maximum; $\mathrm{d}(\overline{u^{2+}})/\mathrm{d}(\log(z^+))$ and $\mathrm{d}^2(\overline{u^{2+}})/\mathrm{d}(\log(z^+))^2$ for NSTAP results as well as DNS of boundary layer (at $Re_\tau = 2500$) are plotted against z^+ in figures 5(*a*) and 5(*b*), respectively. One can see that the zero crossing in $\mathrm{d}^2(\overline{u^{2+}})/\mathrm{d}(\log(z^+))^2$ occurs around $z^+ = 180$ and is a weak function, if not independent, of Re_τ for $Re_\tau = 2500$–20 000. Figure 5(*c*) shows $\mathrm{d}^2\overline{u^{2+}}/\mathrm{d}z^{+2}$, which is proportional to the viscous transport. It appears that the viscous transport is virtually Reynolds number invariant in the intermediate region and becomes zero at nominally $z^+ = 180$. After locating the inflection point, a tangent line is fitted to four to five experimental

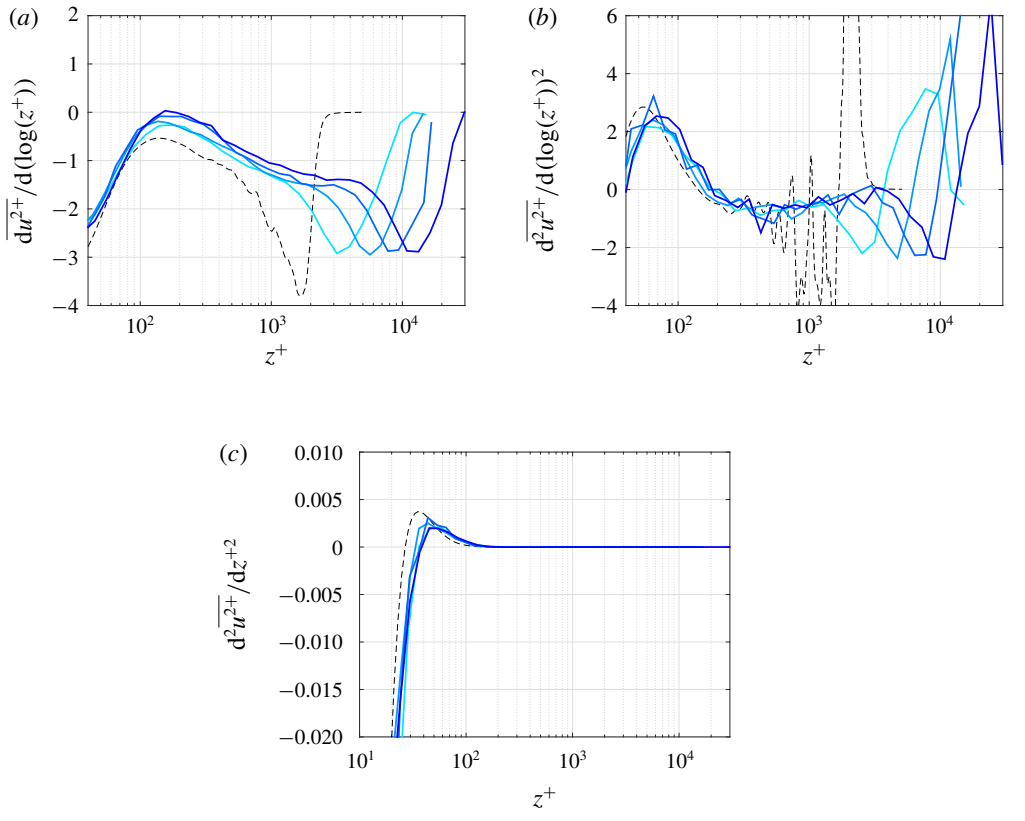

FIGURE 5. (Colour online) (*a*) Inner normalised first derivative of the streamwise turbulence intensity with respect to $\log(z^+)$. (*b*) Inner normalised second derivative of the streamwise turbulence intensity with respect to $\log(z^+)$. (*c*) Inner normalised second derivative of the streamwise turbulence intensity with respect to z^+, which is also proportional to the viscous transport. Lines are as in figure 1.

points in the turbulence intensity profile neighbouring the inflection point with it in the middle, as shown in figure 4. The tangent line is extended in z^+ until it intersects with the logarithmic equation (3.1). The emergence and existence of a second peak in the turbulence intensity with Re_τ is evaluated from the Re_τ scaling of the ordinate and abscissa of the intersection point and the slope of the tangent line. Note that since there is no apparent logarithmic region for $\overline{u^{2+}}$ of the DNS boundary layer we cannot obtain an intersection at this relatively low Re_τ; hence, only the tangent line to the intermediate region is shown in figure 4 for the DNS. Figures 6(*a*) and 6(*b*) show the Re_τ dependence of the intensity (shown by $\overline{u_{p\ int}^{2+}}$) and the viscous-scaled location (shown by $z_{p\ int}^+$) of the intersections, respectively. The Reynolds number dependence of the slope of the tangent logarithmic line S_{int} is shown in figure 6(*c*). It is interesting to see that the slope increases with Re_τ with negative values for low Reynolds numbers, and it crosses zero at $Re_\tau \approx 18\,000$. This trend shows that a hump will eventually emerge in the intermediate region of $\overline{u^{2+}}$ at high Reynolds numbers. Now the intensity and location of the intersection points and the slope values against

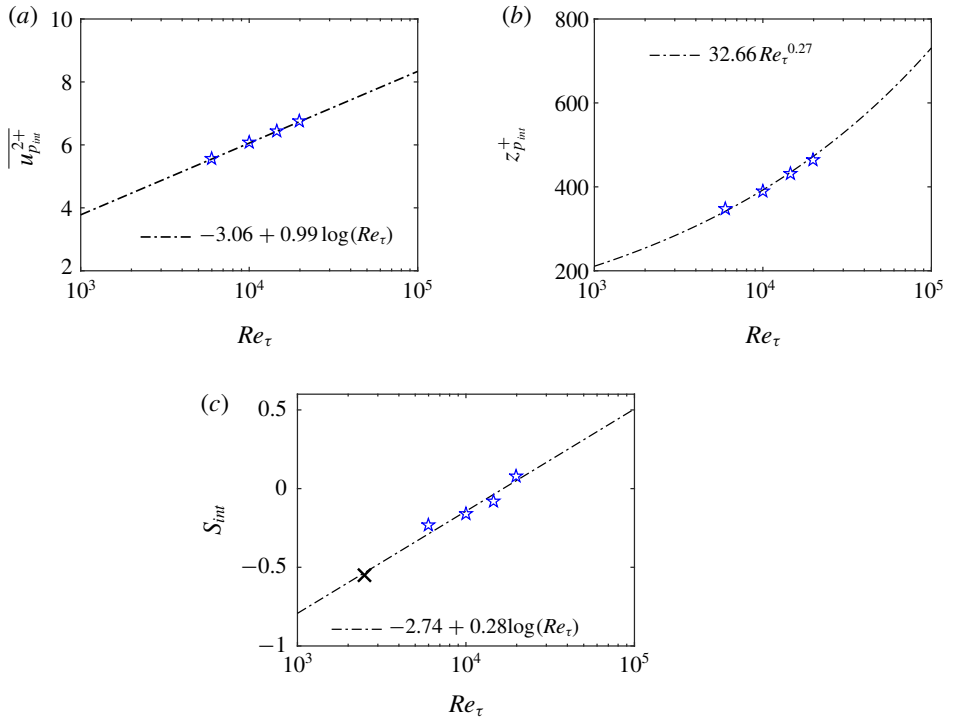

FIGURE 6. (Colour online) Reynolds number dependence of (*a*) the ordinate of the intersection of the tangent line to the turbulence intensity profile at its inflection point with the logarithmic equation (3.1) given by $\overline{u_{p}^{2+}}_{int}$; (*b*) the abscissa of the intersection point given by z^+_{int}; (*c*) the slope of the tangent lines in the intermediate region, S_{int}. ⋆, experimental data from current study; ×, slope of the tangent line to the intermediate region of turbulence intensity profile for the DNS data shown in figure 4(*b*); – · –, curve fits to the intersection values in (*a*) and (*b*) and slope of the logarithmic tangents as a function of Re_τ in (*c*).

Re_τ can be fitted using appropriate functions to obtain

$$\overline{u_{p}^{2+}}_{int} = -3.06 + 0.99\log(Re_\tau), \tag{3.3a}$$

$$z^+_{p\,int} = 32.66 Re_\tau^{0.27}, \tag{3.3b}$$

$$S_{int} = -2.74 + 0.28\log(Re_\tau), \tag{3.3c}$$

which are shown by the dot-dashed lines in figure 6(*a–c*) respectively. It is noted again that the mentioned intersection point is not the second outer peak or the start of the logarithmic region but a geometrical upper bound for the second outer peak. In fact, we are interested in the intermediate region itself rather than the location and value of the outer peak, and the intersection that we find is a reference point from which the logarithmic curve fit to the intermediate region is plotted. The intersection can be determined with more accuracy since locating the outer peak is challenging, particularly for low Reynolds number flows. Marusic *et al.* (2013) used $z^+ = 3Re_\tau{}^{1/2}$ as the lower bound of the logarithmic region and Mathis, Hutchins & Marusic (2010) used $z^+ = 3.9Re_\tau{}^{1/2}$ as the location of the outer peak. Therefore, an exponential

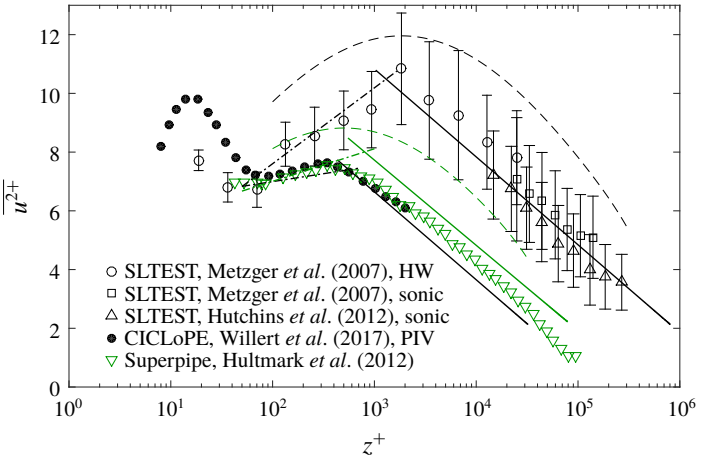

FIGURE 7. (Colour online) Comparison of $\overline{u^{2+}}$ for the SLTEST surface layer (at $Re_\tau \approx 10^6$), Superpipe (at $Re_\tau \approx 10^5$) and CICLoPE pipe experiments (at $Re_\tau \approx 40\,000$) with the logarithmic model of (3.1) (——), the intermediate region correlation of (3.4) (– · –) and the curve fit proposed by Alfredsson *et al.* (2011) (- - - -). The curve fit proposed by Alfredsson *et al.* (2011) is shown for $Re_\tau = 10^5$ and 10^6.

function is used here to find the correlation for the Reynolds number trend of $z^+_{p\ int}$ since it is analogous to the outer peak location.

Having (3.3) one can determine the logarithmic tangent line to the intermediate region for any $Re_\tau \geqslant 6000$ using

$$\overline{u^{2+}} = \overline{u^{2+}_{p}}_{int} + S_{int} \log\left(\frac{z^+}{z^+_{p\ int}}\right). \tag{3.4}$$

Equations (3.3) and (3.4) are used to predict the intermediate region in the turbulence intensity profile for $Re_\tau = 40\,000$, 10^5 and 10^6. This region (shown with dot-dashed lines) together with the logarithmic region (shown with solid lines) for these Reynolds numbers are shown in figure 7, where they are compared with the CICLoPE data from Willert *et al.* (2017) (pipe facility) at $Re_\tau = 40\,000$, Superpipe data from Hultmark *et al.* (2012) at $Re_\tau \approx 10^5$ and the SLTEST data from Metzger *et al.* (2007) and Hutchins *et al.* (2012) at $Re_\tau \sim O(10^6)$. The agreement between the model predictions and the SLTEST data in the intermediate region is very good; moreover, although this model was developed based on the boundary layer data, acceptable agreement is seen between its predictions and the Superpipe and CICLoPE data. Also shown in figure 7 are the curve fits proposed by Alfredsson, Segalini & Örlü (2011) (shown with dashed lines) for $Re_\tau = 10^5$ and 10^6.

Equations (3.2) and (3.3*a*) can be used to predict whether, at sufficiently high Re_τ, the outer peak overcomes the inner peak. The extrapolated results in figure 8 show that such a phenomenon happens around $Re_\tau = 10^8$. Note that since we are using an upper bound for the outer peak, i.e. (3.3*a*), this is a lower bound for the predicted Re_τ. In fact, as recently discussed by Marusic, Baars & Hutchins (2017), if we adopt the near-wall peak slope in (3.2) following a gradient of $A_1/2$ (A_1 is the slope in the logarithmic relation in (3.1)), then the outer peak will never reach the

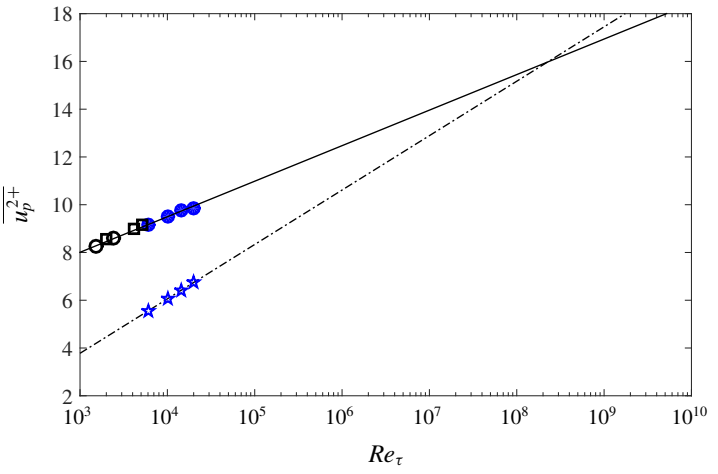

FIGURE 8. (Colour online) Comparison of the Reynolds number dependence of the inner peak given by (3.2) (——) and the ordinate of the intersection of the tangent line to the intermediate region and the log region curve fit given by (3.3*a*) (– · –). Symbols are as in figures 3 and 6.

inner peak. Furthermore, one should acknowledge that these predictions are valid if the inner and the outer peak trends remain unchanged up to these extreme values for Re_τ. Such questions remain controversial since accurate near-wall measurements up to high Re_τ face significant challenges (Morrison *et al.* 2004; Metzger *et al.* 2007; Marusic, Mathis & Hutchins 2010*a*; Hultmark *et al.* 2012). This makes any prospect of this phenomenon tentative. Nonetheless, according to the NSTAP data and the atmospheric surface layer data of Metzger & Klewicki (2001), it is unlikely that this phenomenon happens at laboratory scale or any terrestrial Re_τ.

3.2. *Spatial resolution filtering of turbulence intensity in near-wall region*

Several correction schemes for spatial filtering of single component hot-wire measurements have been proposed recently (Monkewitz, Duncan & Nagib 2010; Chin *et al.* 2011; Segalini *et al.* 2011; Smits *et al.* 2011; Philip *et al.* 2013). Comparisons of these corrections are given by Miller, Estejab & Bailey (2014). Here we restrict our assessment to the correction scheme of Smits *et al.* (2011).

Figure 9 shows $\overline{u^{2+}}$ as measured with the NSTAP and the 2.5 μm diameter hot-wire together with the Smits *et al.* (2011) corrected hot-wire profiles for various Re_τ. It is noted that the NSTAP results are not corrected for spatial resolution since their associated l^+ is small enough to ensure that all the small-scale energy content is resolved. It can be seen that the correction works reasonably well for measurements at $Re_\tau = 6000$, 10 000 and 14 500 where the inner normalised hot-wire length $l_{HW}^+ \approx 20$. However, for $Re_\tau = 20\,000$ with $l_{HW}^+ = 29$, its performance degrades, resulting in an underestimation of the turbulence intensity around the inner peak ($z^+ = 15$). Our results indicate that this correction scheme (validated for up to $Re_\tau = 10\,000$ in the original paper) works well for Re_τ up to at least 14 500 but may not be as accurate for higher Reynolds numbers.

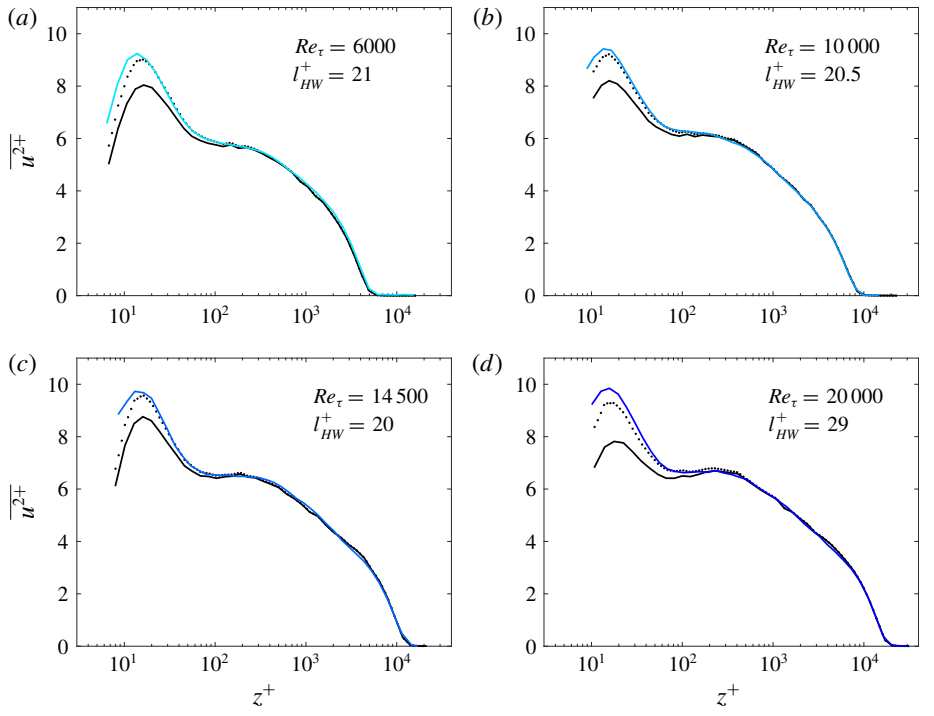

FIGURE 9. (Colour online) Streamwise turbulence intensity measured with the hot-wires and the NSTAP probes at various Re_τ. ——, uncorrected hot-wire data; · · · · · ·, corrected hot-wire data for spatial resolution using the scheme proposed by Smits *et al.* (2011); —, NSTAP, $Re_\tau = 6000$; —, NSTAP, $Re_\tau = 10\,000$; —, NSTAP, $Re_\tau = 14\,500$; —, NSTAP, $Re_\tau = 20\,000$. (*a*) $Re_\tau = 6000$, (*b*) $Re_\tau = 10\,000$, (*c*) $Re_\tau = 14\,500$, (*d*) $Re_\tau = 20\,000$.

3.3. *Skewness and kurtosis*

For completeness we also show skewness (S_u) and kurtosis (K_u) profiles of the streamwise velocity signals against inner-scaled wall distance z^+ in figures 10(*a*) and 10(*b*). In these figures, skewness and kurtosis as measured by the NSTAP and the 2.5 μm diameter conventional hot-wire are compared at various Reynolds numbers. It appears that spatial resolution affects both S_u and K_u in the near-wall region up to $z^+ \approx 200$, but beyond this ($z^+ > 200$) good agreement is observed between the NSTAP and the conventional hot-wire. These results are consistent with the observations of Talamelli *et al.* (2013) about the effect of spatial filtering on the skewness and kurtosis in turbulent wall-bounded flows. It should also be noted that in the skewness profiles, a near-wall negative region (which diminishes with Re_τ) is seen in the NSTAP results for all the Reynolds numbers, while the conventional hot-wire cannot resolve this due to spatial filtering.

3.4. *Energy spectra*

3.4.1. *Near-wall region*

We start this section with a dimensional analysis for the streamwise energy spectrum ϕ_{uu} in the near-wall region. This analysis is similar to that presented by Perry, Henbest & Chong (1986) for the logarithmic wall region; however, we apply it to the near-wall region. The spectrum can be separated into three wavenumber domains.

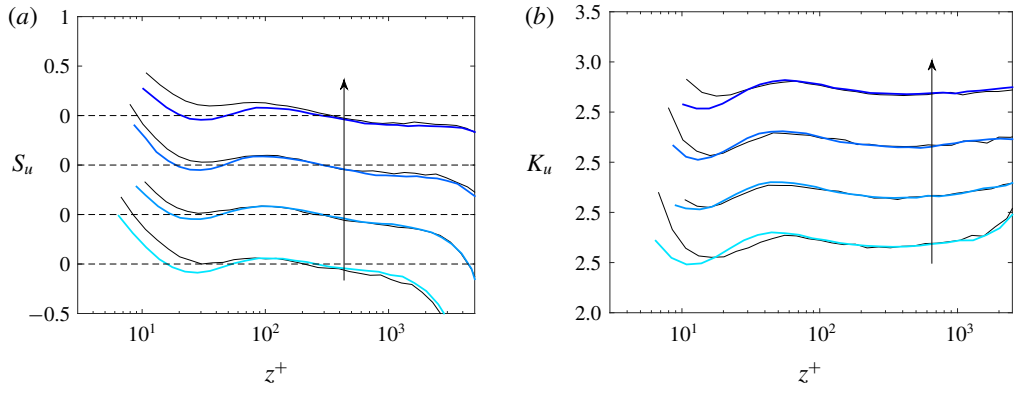

FIGURE 10. (Colour online) Comparison of (*a*) skewness, S_u, and (*b*) kurtosis, K_u, as measured by 2.5 μm diameter hot-wires (——) and the NSTAP at various Re_τ. Reynolds numbers are $Re_\tau = 6000$ (——), 10 000 (——), 14 500 (——) and 20 000 (——) and the arrow direction indicates the increase in Re_τ. Skewness and kurtosis curves have been shifted in the ordinate axis for clarity.

(i) *Small wavenumber (large wavelength) motions*. In this domain, although near the wall, the boundary layer thickness is important since the contributing large-scale motions are of the order of the boundary layer thickness, δ. Hence, the relevant variables are energy spectrum ϕ_{uu}, streamwise wavenumber k_x, friction velocity u_τ, kinematic viscosity ν, wall distance z and boundary layer thickness δ. A dimensional analysis leads to

$$\frac{k_x\phi_{uu}}{u_\tau^2} = f_1(k_x z, z^+, z/\delta) = f_1(k_x^+ z^+, z^+, z^+/\delta^+). \tag{3.5}$$

Equation (3.5) implies that in the near-wall region over the small wavenumber domain, $k_x\phi_{uu}/u_\tau^2$ is dependent on Re_τ as well as k_x^+ and z^+.

(ii) *Moderate to high wavenumber (moderate to small wavelength) motions*. In this wavenumber domain in the near-wall region, the relevant variables are ϕ_{uu}, k_x, u_τ, z and ν. Here, since $z/\delta \ll 1$ for sufficiently high Re_τ, δ is not important. Therefore, a dimensional analysis yields

$$\frac{k_x\phi_{uu}}{u_\tau^2} = f_2(k_x z, z^+) = f_2(k_x^+ z^+, z^+). \tag{3.6}$$

Therefore, in this domain $k_x\phi_{uu}/u_\tau^2$ can be expressed in terms of k^+ and z^+ only.

(iii) *Very high wavenumber (very small wavelength) motions*. In this range of motions, ϕ_{uu} is dependent on wavenumber k_x, Kolmogorov's length scale η and Kolmogorov's velocity scale v_η. Here, $v_\eta = (\nu\epsilon)^{1/4}$ and $\eta = (\nu^3/\epsilon)^{1/4}$, where ν is kinematic viscosity and ϵ is the dissipation rate. With these variables two non-dimensional parameters can be considered such that

$$\frac{k_x\phi_{uu}}{v_\eta^2} = f_3(k_x\eta) = f_3(k_x^+\eta^+). \tag{3.7}$$

It is shown in appendix B that in the near-wall region and the inertial sublayer, η^+ and v_η^+ can be expressed as functions of inner normalised wall distance z^+,

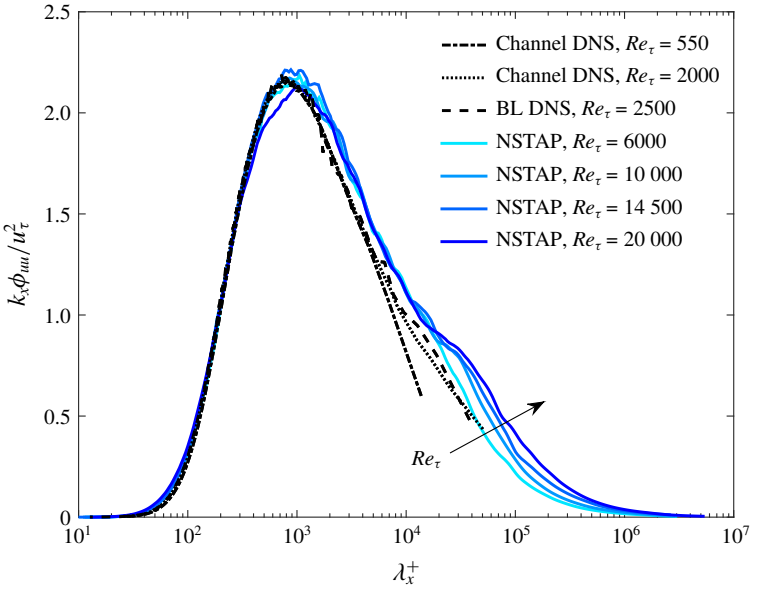

FIGURE 11. (Colour online) Comparison of pre-multiplied energy spectra at $z^+ \approx 15$ from various Reynolds numbers and flow geometries. The arrow indicates increase in Re_τ for the NSTAP spectra.

independent of Re_τ, i.e. $\eta^+ = h_\eta(z^+)$ and $v_\eta^+ = h_v(z^+)$. Therefore, equation (3.7) can be rewritten as

$$\frac{k_x\phi_{uu}}{u_\tau^2} = [h_v(z^+)]^2 f_3(k_x^+ h_\eta(z^+)), \tag{3.8}$$

which shows that in this wavenumber domain, similar to moderate to high wavenumber motions, $k_x\phi_{uu}/u_\tau^2$ is a function of k^+ and z^+ and independent of Re_τ.

The above arguments indicate that at a fixed z^+ in the near wall, $k_x\phi_{uu}(k^+)/u_\tau^2$ (or equivalently $k_x\phi_{uu}(\lambda_x^+)/u_\tau^2$ where $\lambda_x = 2\pi/k_x$ is the wavelength) curves should collapse over medium to very high wavenumbers (medium to very low wavelengths) when various Re_τ are compared, and Re_τ dependence is expected in the low wavenumber (high wavelength) end of the spectra only. Since small-scale energy can be significantly affected by spatial resolution (as documented by Chin *et al.* (2009) and Hutchins *et al.* (2009)), the data here may be helpful to clarify the small-scale behaviour in the near wall. The inner-scaled, pre-multiplied energy spectra $k_x\phi_{uu}/u_\tau^2$ are plotted against streamwise wavelength, λ_x^+, in figure 11 at the peak turbulence intensity location, $z^+ \approx 15$ for the experimental data ($Re_\tau = 6000$, 10 000, 14 500 and 20 000) as well as channel DNS data of Hoyas & Jiménez (2006) at $Re_\tau = 550$, 2000 and boundary layer DNS data of Sillero *et al.* (2013) at $Re_\tau = 2500$. Taylor's frozen turbulence hypothesis (Taylor 1938) is employed to deduce spatial spectra from the time series data obtained from the stationary hot-wire for the experimental spectra, while spatial information is used to construct spectra from DNS. Here, spectra are plotted in pre-multiplied form so that equal areas equate to equal contributions to the turbulence intensities on the semilogorithmic plot: $\int_0^\infty \phi_{uu}\,\mathrm{d}k_x = \int_0^\infty k_x\phi_{uu}\,\mathrm{d}(\log k_x) = \int_0^\infty k_x\phi_{uu}\,\mathrm{d}(\log \lambda_x) = \overline{u^2}$.

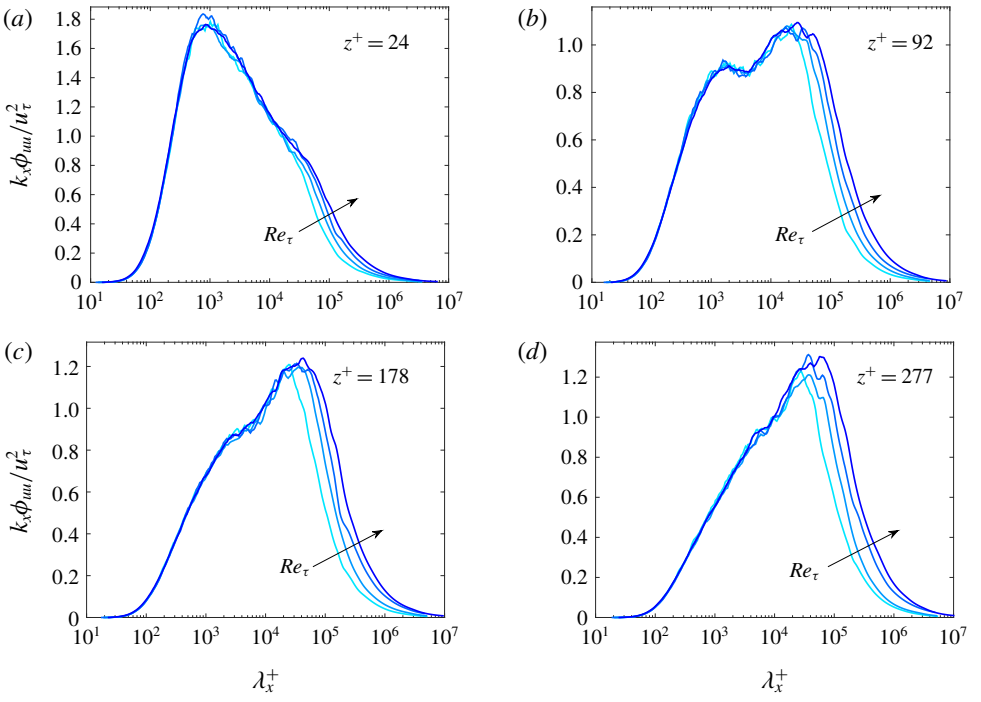

FIGURE 12. (Colour online) Reynolds number dependence of pre-multiplied energy spectra as measured with the NSTAP at (*a*) $z^+ \approx 24$, (*b*) $z^+ \approx 92$, (*c*) $z^+ \approx 180$, (*d*) $z^+ \approx 280$. Lines are as in figure 11. The arrow indicates increase in Re_τ.

All the spectra appear to collapse well for the wavelengths below $\lambda_x^+ \approx 700$ and the experimental spectra ($Re_\tau \geqslant 6000$) collapse well for the wavelengths below $\lambda_x^+ \approx 15\,000$. This is consistent with the dimensional analysis. Moreover, in the high wavelength end of the spectra an increasing trend with Re_τ is evident. These observations are consistent with the experimental study of Hutchins *et al.* (2009) in the boundary layer flow (up to $Re_\tau \approx 19\,000$) where hot-wire sensors with lengths of 22 wall units were used, and for the lower Reynolds number DNS studies of Hoyas & Jiménez (2006) (up to $Re_\tau \approx 2000$) in the channel flow, and Chin, Monty & Ooi (2014) (up to $Re_\tau \approx 2000$) in the pipe flow. It is not clear why the DNS and the experimental spectra diverge for $10^3 < \lambda_x^+ < 10^4$. This may be due to use of Taylor's frozen turbulence hypothesis in experimental spectra. The peak of the inner normalised pre-multiplied energy spectra is seen to remain constant at $k_x\phi_{uu}/u_\tau^2 \approx 2.2$ at the inner normalised wavelength $\lambda_x^+ \approx 850$ within measurement uncertainty. It should also be noted that the small-scale energy is not only invariant with Re_τ but independent of the flow geometry, since channel and boundary layer flow spectra in the small-scale region appear to collapse well. This behaviour in the u-spectra at $z^+ \approx 15$ explains the increasing trend with Re_τ for the peak $\overline{u^{2+}}$ in the near-wall region; there is an increasing amount of large-scale superimposed energy as Re_τ increases while the small-scale energy content appears to be universal. Figure 12 shows the same plots for the experimental data at other inner normalised wall distance locations. It can be seen that the $k_x\phi_{uu}/u_\tau^2$ curves collapse for wavelengths below $\lambda_x^+ \approx 15\,000$ up to $z^+ = 280$ for the Reynolds number range $6000 \leqslant Re_\tau \leqslant 20\,000$.

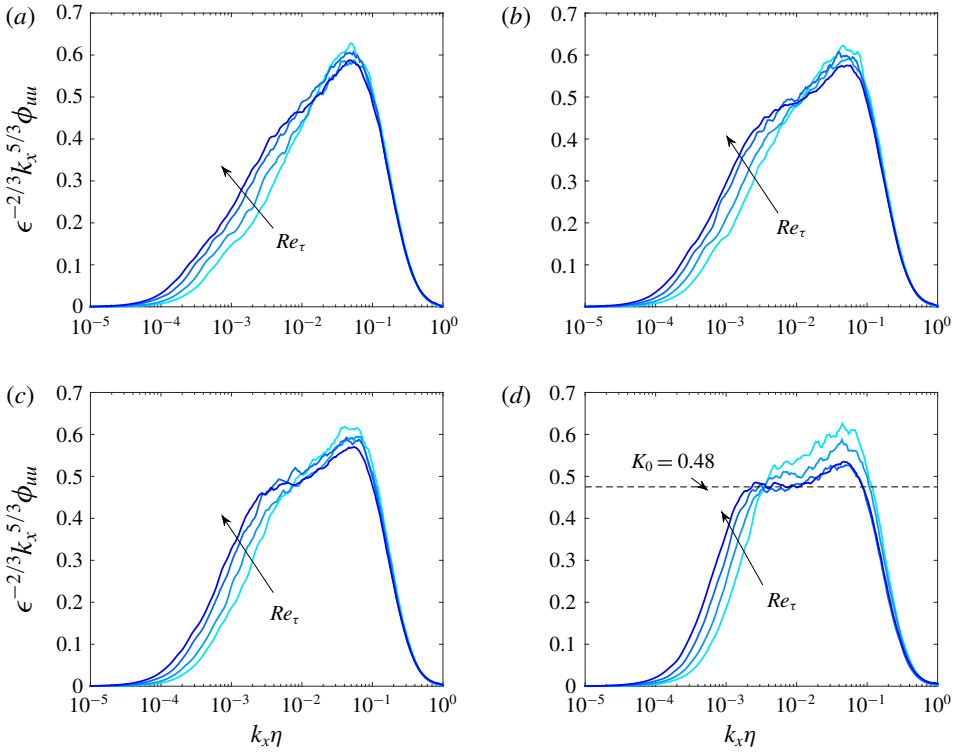

FIGURE 13. (Colour online) Compensated Kolmogorov's universal scaling for the streamwise energy spectra at $Re_\tau = 6000,\ 10\,000,\ 14\,500,\ 20\,000$ at (*a*) $z/\delta \approx 0.05$, (*b*) $z/\delta \approx 0.1$, (*c*) $z/\delta \approx 0.15$, (*d*) $z/\delta \approx 0.4$. Saddoughi & Veeravalli (1994) found the Kolmogorov constant to be $K_0 = 0.49$, which is slightly higher than our result which is $K_0 = 0.48$. The arrow indicates increase in Re_τ.

3.4.2. *The $k_x^{-5/3}$ power scaling law*

Hutchins *et al.* (2009) have shown that limited spatial resolution of hot-wires can affect the $k_x^{-5/3}$ power scaling region by attenuating the so-called 'spectral bump' in the Kolmogorov-scaled energy spectra (Saddoughi & Veeravalli 1994), resulting in misleading estimates of $-5/3$ regions. Here, the NSTAP length is shorter than the Kolmogorov length scale in the logarithmic and outer regions where $k_x^{-5/3}$ power scaling is expected to hold (see figure 17(*a*) for inner normalised Kolmogorov length scale values across the boundary layer thickness at varying Re_τ); hence, we inspect this scaling across a range of Reynolds numbers in turbulent boundary layers. The mean rate of turbulent kinetic energy dissipation (ϵ) is estimated using local isotropy, which allows ϵ to be determined from integration of the one-dimensional dissipation spectrum $D(k_x)$ (Townsend 1976), i.e.

$$\epsilon = 15\nu \int_0^\infty D(k_x)\,\mathrm{d}k_x = 15\nu \int_0^\infty k_x^2 \phi_{uu}\,\mathrm{d}k_x. \tag{3.9}$$

Figure 13 shows the compensated Kolmogorov-scaled streamwise energy spectra at four outer-scaled wall-normal locations for various Reynolds numbers. The $-5/3$ scaling law appears as a horizontal line in this form of compensated spectra. One can

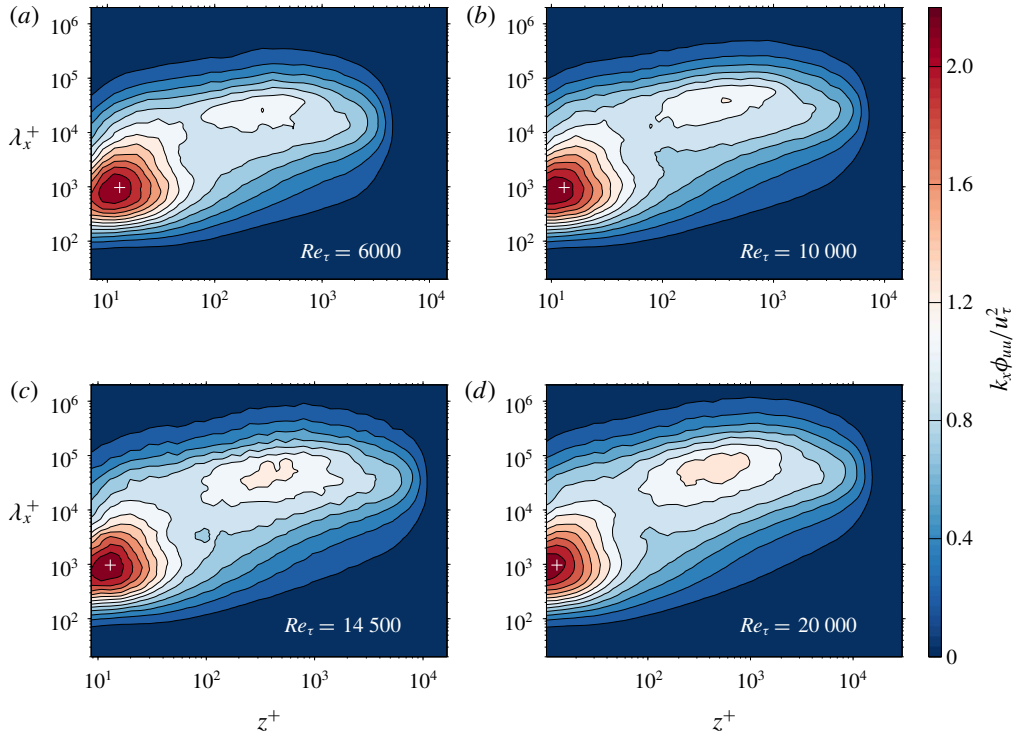

FIGURE 14. (Colour online) Pre-multiplied spectra for the streamwise velocity $k_x\phi_{uu}/u_\tau$ against inner-scaled wavelength λ_x^+ and wall distance z^+ at (*a*) $Re_\tau = 6000$, (*b*) $Re_\tau = 10\,000$, (*c*) $Re_\tau = 14\,500$ and (*d*) $Re_\tau = 20\,000$. '+' indicates the inner energy site.

see that a clear $-5/3$ scaling is elusive for $z/\delta \leqslant 0.15$, i.e. the logarithmic region, in the Re_τ range of this study. Only at $z/\delta = 0.4$, which is located in the wake region, are apparent regions of plateau observed. Vallikivi *et al.* (2015*a*), however, found that for high Reynolds number turbulent boundary layer and pipe flows at $z/\delta = 0.5$, energy spectra have an exponent that is closer to -1.5 than to $-5/3$. The plateau level in our results, which equates to Kolmogorov's constant K_0, changes with Re_τ from 0.52 for $Re_\tau = 6000$ to 0.48 for $Re_\tau = 14\,500$ and $20\,000$ (the plateau values are determined by fitting a horizontal line to the flat portions of the compensated spectra at $z/\delta = 0.4$). This is probably because in the lower Re_τ cases, the separation between large energetic scales and small dissipative scales is insufficient. The Kolmogorov constant for the highest Re_τ ($K_0 = 0.48$) is slightly lower than that reported by Saddoughi & Veeravalli (1994) ($K_0 = 0.49$) in their extremely high-Re_τ boundary layer experiment. This insufficient scale separation might be part of the reason for the weak Reynolds number dependence of the Kolmogorov constant reported in the literature (Sreenivasan 1995).

3.4.3. *Spectrograms*

In an attempt to provide an overview of the energy distribution across various wavelengths and wall distances, and also the effect of Re_τ on the energy distribution, contour maps of the pre-multiplied energy spectra $k_x\phi_{uu}/u_\tau^2$ are plotted against inner-scaled wall distance (z^+) and inner-scaled streamwise wavelength in figure 14

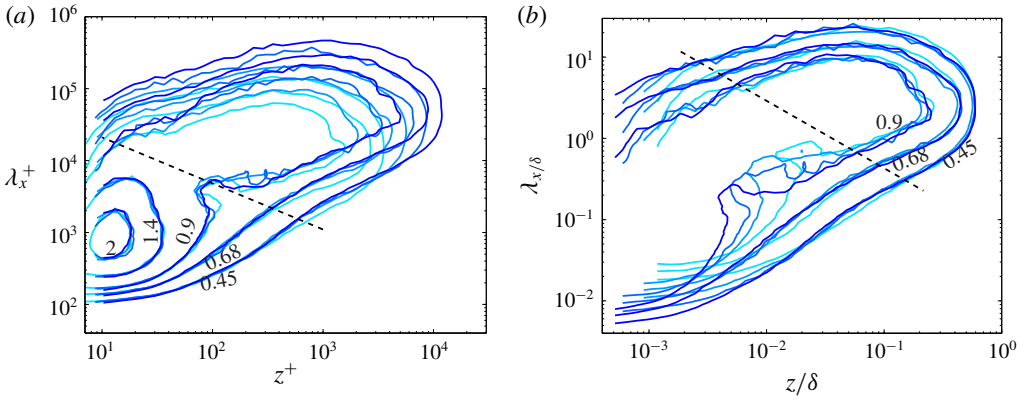

FIGURE 15. (Colour online) Iso-contours of $k_x\phi_{uu}/u_\tau^2$ against (*a*) inner-scaled wavelength λ_x^+ and wall distance z^+ at the contour levels of 2, 1.4, 0.9, 0.68 and 0.45, (*b*) δ-scaled wave length λ_x/δ and wall distance z/δ at the contour levels of 0.9, 0.68 and 0.45 for various Re_τ. Reynolds numbers are 6000 (—), 10 000 (—), 14 500 (—) and 20 000 (—).

for $Re_\tau = 6000$–$20\,000$. Here the magnitude of $k_x\phi_{uu}/u_\tau^2$ is indicated using colour variations. These contour maps show a distinct near-wall peak in the spectrogram for all Reynolds numbers (indicated with white '+' symbols) known as the 'inner energy site', which occur at a nominally fixed inner-scaled wall distance $z^+ \approx 13$ and inner-scaled wavelength $\lambda_x^+ \approx 1000$ at a fixed energy level $k_x\phi_{uu}/u_\tau^2 \approx 2.2$. This wall distance corresponds to approximately the peak in the broadband turbulence intensity, and is related to the near-wall energetic cycle of streaks and quasi-streamwise vortices (Kline *et al.* 1967; Jiménez & Pinelli 1999). In order to acquire better comprehension of the Re_τ effect on the near-wall energy spectral density, iso-contours of pre-multiplied energy for the spectral surfaces shown previously are now shown in figure 15(*a*) for various Re_τ. Five contour levels corresponding to $k_x\phi_{uu}/u_\tau^2 = 0.45$, 0.68, 0.9, 1.4 and 2 are shown, and colour gradients are used to indicate Re_τ variations. The four sets of contours (four Reynolds numbers) show very good collapse on the left-hand side of the inclined dashed line. However, if we look to the right of the dashed line, it is evident that there is an increasing amount of high wavelength energy with Re_τ extending across all wall heights. This high wavelength energy in the near-wall region is the footprint of an emergent 'outer energy site', growth of which with Re_τ is evident in figure 14. Hutchins & Marusic (2007) reported emergence of an outer peak associated with this outer energy site at higher Reynolds numbers, and Mathis, Hutchins & Marusic (2009) later proposed the location of the peak to be Re_τ dependent as $z^+ \approx \sqrt{15Re_\tau}$, which coincides with the geometric centre of the logarithmic region. More recently, Vallikivi *et al.* (2015*a*) reported that the location of the outer spectral peak at high Reynolds numbers marks the start of a broad plateau. This latter observation is consistent with the outer spectral region at $Re_\tau = 20\,000$ in our results. However, $Re_\tau = 20\,000$ is only sufficient to see the emergence of this broad plateau which would be expected from the results of Vallikivi *et al.* (2015*a*) to become more prominent at higher Reynolds numbers. Figure 15(*b*) shows a Reynolds number comparison of three contour levels corresponding to $k_x\phi_{uu}/u_\tau^2 = 0.45$, 0.68, 0.9 against outer-scaled wavelength and wall distance. It is evident that the outer-scaled spectra collapse well in the outer region

(showing existence of an outer-scaling similarity) and gradually separate at lower z/δ and λ_x/δ. This is consistent with the attached eddy hypothesis model of Perry *et al.* (1986).

4. Conclusions

Nano-scale thermal anemometry probes (NSTAPs) were employed to measure the streamwise velocity fluctuations in the large University of Melbourne wind tunnel in the Reynolds number range $Re_\tau = 6000$–$20\,000$. This enabled viscous-scaled sensor lengths in the range $l^+ = 2.4$–3.5, ensuring that all the energetic small scales in the near-wall region are resolved. To validate the NSTAPs, several measurement repeats at each Reynolds number were performed, and mean velocity U and streamwise turbulence intensity $\overline{u^2}$ as measured by the NSTAPs were compared with those measured by conventional 2.5 μm diameter hot-wires, which were used as baselines. Those NSTAPs that agreed with the 2.5 μm diameter hot-wires in the logarithmic and outer regions of $\overline{u^2}$ were deemed reliable and their results were averaged to obtain the averaged NSTAP results at each Re_τ. NSTAP results revealed that in the near-wall region the streamwise turbulence intensity normalised with u_τ ($\overline{u^{2+}}$) increases monotonically with Re_τ in the Reynolds number range of the experiments, and the near-wall peak in $\overline{u^{2+}}$ was found to follow a log–linear relation with Re_τ consistent with that recently reported from various DNS results by Lee & Moser (2015). Moreover, profiles of $\overline{u^{2+}}$ against outer-scaled wall distance z/δ in the logarithmic and outer regions collapsed well, following a logarithmic decay of the form $\overline{u^{2+}} = B_1 - A_1 \log(z/\delta)$, with $A_1 = 1.26$ and $B_1 = 1.95$ in the logarithmic region. A logarithmic curve fit was proposed for the intermediate region ($100 \leqslant z^+ \leqslant 3.9Re_\tau^{1/2}$) of the turbulence intensity profile. Extrapolating the fit showed a clear outer peak at Reynolds number $Re_\tau = O(10^6)$, exhibiting very good agreement with atmospheric surface layer data. A correction scheme for $\overline{u^{2+}}$ acquired with insufficient spatial resolution by Smits *et al.* (2011) was used to correct 2.5 μm diameter hot-wire data and comparison was made with those from the NSTAPs. This revealed a good performance of the correction scheme up to $Re_\tau = 14\,500$; however, at $Re_\tau = 20\,000$ (for the hot-wire viscous-scaled length $l^+_{HW} = 29$) the corrected turbulence intensity profile slightly underestimated the fully resolved counterpart measured by the NSTAP. Skewness and kurtosis as measured by the NSTAP and conventional hot-wires were compared at various Reynolds numbers and it was shown that finite hot-wire length affects these profiles only in the viscous-scaled wall height range $z^+ < 200$ for $l^+ \leqslant 29$.

Streamwise velocity energy spectra were investigated in the near-wall region ($z^+ \leqslant 300$). Consistent with dimensional analysis, the energy spectra in the near-wall region were found to be functions of only inner normalised wall distance and wavenumber, in the very high to moderate wavenumbers range. This was confirmed by fully resolved experimental spectra. When u-spectra of various Reynolds numbers from experiment were compared at fixed viscous-scaled wall distances, in the near-wall region ($z^+ \leqslant 300$) inner-scaling collapsed the spectra for small to moderate wavelengths (large to moderate wavenumbers), while the spectra exhibited an increasing trend with Re_τ for large wavelengths. These large-scale energy contributions in the u-spectra, which increase with Re_τ, are attributed to the footprint of large-scale features in the inertial sublayer, and are responsible for the growth of the turbulence intensity inner peak with Re_τ.

A Reynolds number comparison of compensated Kolmogorov-scaled u-spectra was also made at different wall distances, showing that there is no clear $-5/3$ scaling in the energy spectra within the logarithmic region for turbulent boundary layer flows in the Reynolds number range $Re_\tau = 6500$–$20\,000$. Only in the wake region, namely at $z/\delta = 0.4$, was an apparent plateau in the compensated Kolmogorov-scaled spectra for the higher Reynolds number cases ($Re_\tau = 14\,500$ and $20\,000$) observed with the Kolmogorov constant $K_0 = 0.48$, consistent with that reported by Saddoughi & Veeravalli (1994).

Finally, pre-multiplied u-spectra, $k_x\phi_{uu}$, as contour plots were analysed with different scalings. Comparison of the spectra against inner-scaled wavelength λ_x^+ and wall distance z^+ depicted a clear near-wall peak (with the energy level $k_x\phi_{uu} \approx 2.2$) associated with the near-wall peak in $\overline{u^{2+}}$ for various Reynolds numbers. Iso-contours of pre-multiplied energy for the spectral surfaces were compared for various Reynolds numbers in viscous and δ scaling. It was shown that the spectra of various Re_τ with viscous scaling collapse in the near-wall region for low to moderate wavelengths, while δ-scaled iso-countours collapsed in the outer region over moderate to high wavelengths.

Acknowledgements

The authors gratefully acknowledge the financial support of the Australian Research Council. M.K.F. was supported by the Department of Defense (DoD) through the National Defense Science & Engineering Graduate Fellowship (NDSEG) Program. This material is based upon work supported by the National Science Foundation under grant CBET-1510100 (programme manager Ron Joslin).

Appendix A

Here we describe the procedure carried out to validate the NSTAP probes. Several NSTAP probes together with 2.5 μm diameter hot-wires were used for the measurement of streamwise velocity fluctuations at each Reynolds number. Mean velocity U and streamwise turbulence intensity $\overline{u^2}$ as measured by the NSTAPs were compared to those measured by the hot-wires. These comparisons are shown in figure 16, only for $Re_\tau = 20\,000$, as an example. The mean velocity profiles measured by all the NSTAPs agree with that measured by the standard hot-wire; however, comparison of the turbulence intensity profiles revealed discrepancies between some of the NSTAPs and the hot-wires in the logarithmic and outer region. Hutchins *et al.* (2009) have shown that the effect of spatial resolution in the logarithmic and outer region of the streamwise turbulence intensity profile acquired with hot-wires with viscous-scaled length up to $l^+ \approx 150$ is minimal. This can be explained by the fact that the energy-containing motions in these regions are of the order of the boundary layer thickness, which is normally orders of magnitude larger than the conventional hot-wires in large facilities like the one used in the current study. Hence, we expect to observe minimal difference between NSTAP and 2.5 μm diameter hot-wire in the logarithmic and outer region, despite better spatial resolution of the NSTAP. Those NSTAPs that are in agreement with the 2.5 μm diameter hot-wire in the logarithmic and outer region of $\overline{u^{2+}}$ are deemed reliable, and their results are averaged to obtain the averaged NSTAP statistics and energy spectra at each Reynolds number. The anomalous behaviour of individual NSTAP sensors is consistent with a resonance peak in the Dantec-NSTAP response. This resonance was not observed in the still air

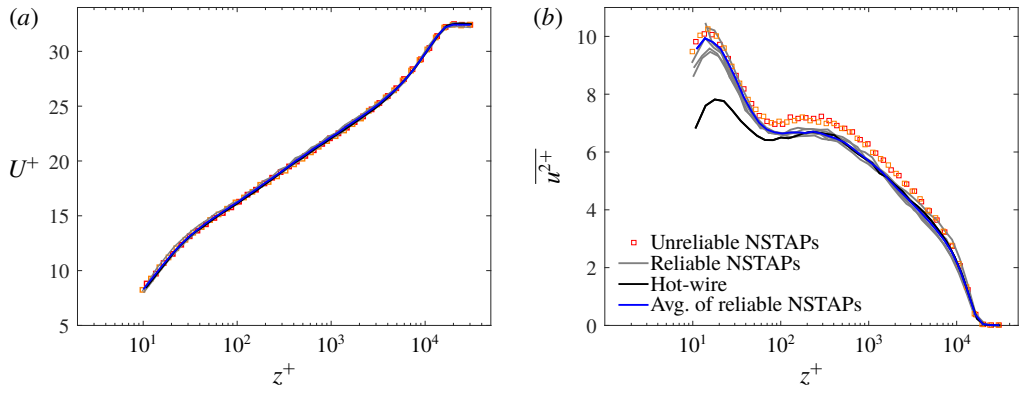

FIGURE 16. (Colour online) Validation of the NSTAP. (*a*) Inner normalised streamwise mean velocity, U^+, against inner normalised wall distance, z^+. (*b*) Inner normalised streamwise turbulence intensity, $\overline{u^{2+}}$, against z^+.

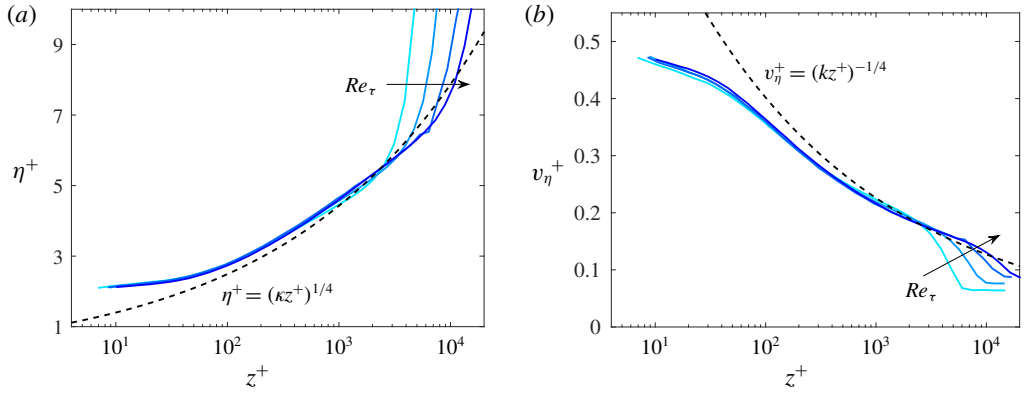

FIGURE 17. (Colour online) (*a*) Inner normalised Kolmogorov length scale, η^+, and (*b*) inner normalised Kolmogorov velocity scale, v_η^+, against z^+ at $Re_\tau = 6000$, 10 000, 14 500 and 20 000. Dashed lines correspond to approximation equations $\eta^+ = (\kappa z^+)^{1/4}$ in (*a*) and $v_\eta^+ = (\kappa z^+)^{-1/4}$ in (*b*) obtained from balancing production and dissipation in logarithmic region (Perry *et al.* 1986). The arrows indicate increase in Re_τ.

square wave response, but could be present in higher velocity flow. Such behaviour was observed only in a small number of wires. Characterisation of this behaviour was limited by the operating parameters of the Dantec system and remains an open topic for further investigation.

Appendix B

Figure 17 shows the inner normalised Kolmogorov length scale (η^+) and velocity scale (v_η^+) against inner normalised wall distance (z^+) for various Reynolds numbers from the well-resolved NSTAP measurements. To estimate η^+ and v_η^+ an estimate of the mean rate of dissipation of the turbulent kinetic energy (ϵ) is required. This is achieved with the aid of local isotropy assumption, which permits estimation of ϵ by integrating the dissipation spectra using (3.9). One can see in figure 17 that both η^+ and v_η^+ exhibit good collapse for $z^+ \leqslant 500$.

REFERENCES

ALFREDSSON, P. H., SEGALINI, A. & ÖRLÜ, R. 2011 A new scaling for the streamwise turbulence intensity in wall-bounded turbulent flows and what it tells us about the 'outer' peak. *Phys. Fluids* **23** (4), 041702.

BAARS, W. J., SQUIRE, D. T., TALLURU, K. M., ABBASSI, M. R., HUTCHINS, N. & MARUSIC, I. 2016 Wall-drag measurements of smooth- and rough-wall turbulent boundary layers using a floating element. *Exp. Fluids* **57** (5), 90.

BAILEY, S. C. C., KUNKEL, G. J., HULTMARK, M., VALLIKIVI, M., HILL, J. P., MEYER, K. A., TSAY, C., ARNOLD, C. B. & SMITS, A. J. 2010 Turbulence measurements using a nanoscale thermal anemometry probe. *J. Fluid Mech.* **663**, 160–179.

CHAUHAN, K. A., MONKEWITZ, P. A. & NAGIB, H. M. 2009 Criteria for assessing experiments in zero pressure gradient boundary layers. *Fluid Dyn. Res.* **41** (2), 021404.

CHIN, C. C., HUTCHINS, N., OOI, A. & MARUSIC, I. 2009 Use of direct numerical simulation (DNS) data to investigate spatial resolution issues in measurements of wall-bounded turbulence. *Meas. Sci. Technol.* **20** (11), 115401.

CHIN, C. C., HUTCHINS, N., OOI, A. & MARUSIC, I. 2011 Spatial resolution correction for hot-wire anemometry in wall turbulence. *Exp. Fluids* **50** (5), 1443–1453.

CHIN, C. C., MONTY, J. P. & OOI, A. 2014 Reynolds number effects in DNS of pipe flow and comparison with channels and boundary layers. *Intl J. Heat Fluid Flow* **45**, 33–40.

COLEMAN, H. W & STEELE, W. G. 2009 *Experimentation, Validation, and Uncertainty Analysis for Engineers*. Wiley.

DE GRAAFF, D. B. & EATON, J. K. 2000 Reynolds-number scaling of the flat-plate turbulent boundary layer. *J. Fluid Mech.* **422**, 319–346.

FERNHOLZ, H. H. & FINLEY, P. J. 1996 The incompressible zero-pressure-gradient turbulent boundary layer: an assessment of the data. *Prog. Aerosp. Sci.* **32** (4), 245–311.

HOYAS, S. & JIMÉNEZ, J. 2006 Scaling of the velocity fluctuations in turbulent channels up to $Re_\tau = 2003$. *Phys. Fluids* **18** (1), 011702.

HULTMARK, M. & SMITS, A. J. 2010 Temperature corrections for constant temperature and constant current hot-wire anemometers. *Meas. Sci. Technol.* **21** (10), 105404.

HULTMARK, M., VALLIKIVI, M., BAILEY, S. C. C. & SMITS, A. J. 2012 Turbulent pipe flow at extreme Reynolds numbers. *Phys. Rev. Lett.* **108** (9), 094501.

HULTMARK, M., VALLIKIVI, M., BAILEY, S. C. C. & SMITS, A. J. 2013 Logarithmic scaling of turbulence in smooth- and rough-wall pipe flow. *J. Fluid Mech.* **728**, 376–395.

HUTCHINS, N., CHAUHAN, K., MARUSIC, I., MONTY, J. P. & KLEWICKI, J. 2012 Towards reconciling the large-scale structure of turbulent boundary layers in the atmosphere and laboratory. *Boundary-Layer Meteorol.* **145** (2), 273–306.

HUTCHINS, N. & MARUSIC, I. 2007 Evidence of very long meandering features in the logarithmic region of turbulent boundary layers. *J. Fluid Mech.* **579**, 1–28.

HUTCHINS, N., NICKELS, T. B., MARUSIC, I. & CHONG, M. S. 2009 Hot-wire spatial resolution issues in wall-bounded turbulence. *J. Fluid Mech.* **635**, 103–136.

JIMÉNEZ, J. & PINELLI, A. 1999 The autonomous cycle of near-wall turbulence. *J. Fluid Mech.* **389**, 335–359.

KLEWICKI, J. C. & FALCO, R. E. 1990 On accurately measuring statistics associated with small-scale structure in turbulent boundary layers using hot-wire probes. *J. Fluid Mech.* **219**, 119–142.

KLINE, S. J., REYNOLDS, W. C., SCHRAUB, F. A. & RUNSTADLER, P. W. 1967 The structure of turbulent boundary layers. *J. Fluid Mech.* **30** (4), 741–773.

LEE, M. & MOSER, R. D. 2015 Direct numerical simulation of turbulent channel flow up to $Re_\tau \approx 5200$. *J. Fluid Mech.* **774**, 395–415.

LIGRANI, P. M. & BRADSHAW, P. 1987 Spatial resolution and measurement of turbulence in the viscous sublayer using subminiature hot-wire probes. *Exp. Fluids* **5** (6), 407–417.

LOZANO-DURÁN, A. & JIMÉNEZ, J. 2014 Effect of the computational domain on direct simulations of turbulent channels up to $Re_\tau = 4200$. *Phys. Fluids* **26** (1), 011702.

MARUSIC, I., BAARS, W. J. & HUTCHINS, N. 2017 Scaling of the streamwise turbulence intensity in the context of inner–outer interactions in wall turbulence. *Phys. Rev. Fluids* **2** (10), 100502.

MARUSIC, I., CHAUHAN, K. A., KULANDAIVELU, V. & HUTCHINS, N. 2015 Evolution of zero-pressure-gradient boundary layers from different tripping conditions. *J. Fluid Mech.* **783**, 379–411.

MARUSIC, I., MATHIS, R. & HUTCHINS, N. 2010*a* High Reynolds number effects in wall turbulence. *Intl J. Heat Fluid Flow* **31** (3), 418–428.

MARUSIC, I., MCKEON, B. J., MONKEWITZ, P. A., NAGIB, H. M., SMITS, A. J. & SREENIVASAN, K. R. 2010*b* Wall-bounded turbulent flows at high Reynolds numbers: recent advances and key issues. *Phys. Fluids* **22** (6), 065103.

MARUSIC, I., MONTY, J. P., HULTMARK, M. & SMITS, A. J. 2013 On the logarithmic region in wall turbulence. *J. Fluid Mech.* **716**, R3.

MATHIS, R., HUTCHINS, N. & MARUSIC, I. 2009 Large-scale amplitude modulation of the small-scale structures in turbulent boundary layers. *J. Fluid Mech.* **628**, 311–337.

MATHIS, R., HUTCHINS, N. & MARUSIC, I. 2010 Scaling of inner and outer regions for flat plate boundary layers. In *Proceedings of the 17th Australasian Fluid Mechanics Conference, Auckland, New Zealand*, pp. 5–9.

METZGER, M. M. & KLEWICKI, J. C. 2001 A comparative study of near-wall turbulence in high and low Reynolds number boundary layers. *Phys. Fluids* **13** (3), 692–701.

METZGER, M. M., KLEWICKI, J. C., BRADSHAW, K. L. & SADR, R. 2001 Scaling the near-wall axial turbulent stress in the zero pressure gradient boundary layer. *Phys. Fluids* **13** (6), 1819–1821.

METZGER, M. M., MCKEON, B. J. & HOLMES, H. 2007 The near-neutral atmospheric surface layer: turbulence and non-stationarity. *Phil. Trans. R. Soc. Lond.* A **365** (1852), 859–876.

MILLER, M. A., ESTEJAB, B. & BAILEY, S. C. C. 2014 Evaluation of hot-wire spatial filtering corrections for wall turbulence and correction for end-conduction effects. *Exp. Fluids* **55** (5), 1735.

MOCHIZUKI, S. & NIEUWSTADT, F. T. M. 1996 Reynolds-number-dependence of the maximum in the streamwise velocity fluctuations in wall turbulence. *Exp. Fluids* **21** (3), 218–226.

MONKEWITZ, P. A., DUNCAN, R. D. & NAGIB, H. M. 2010 Correcting hot-wire measurements of stream-wise turbulence intensity in boundary layers. *Phys. Fluids* **22** (9), 091701.

MORRISON, J. F., MCKEON, B. J., JIANG, W. & SMITS, A. J. 2004 Scaling of the streamwise velocity component in turbulent pipe flow. *J. Fluid Mech.* **508**, 99–131.

NICKELS, T. B., MARUSIC, I., HAFEZ, S. & CHONG, M. S. 2005 Evidence of the k_1^{-1} law in a high-Reynolds-number turbulent boundary layer. *Phys. Rev. Lett.* **95** (7), 074501.

ÖRLÜ, R., FIORINI, T., SEGALINI, A., BELLANI, G., TALAMELLI, A. & ALFREDSSON, P. H. 2017 Reynolds stress scaling in pipe flow turbulence: first results from CICLoPE. *Phil. Trans. R. Soc. Lond.* A **375** (2089), 20160187.

PERRY, A. E., HENBEST, S. & CHONG, M. S. 1986 A theoretical and experimental study of wall turbulence. *J. Fluid Mech.* **165**, 163–199.

PHILIP, J., HUTCHINS, N., MONTY, J. P. & MARUSIC, I. 2013 Spatial averaging of velocity measurements in wall-bounded turbulence: single hot-wires. *Meas. Sci. Technol.* **24** (11), 115301.

PIOMELLI, U. & BALARAS, E. 2002 Wall-layer models for large-eddy simulations. *Annu. Rev. Fluid Mech.* **34** (1), 349–374.

ROSENBERG, B. J., HULTMARK, M., VALLIKIVI, M., BAILEY, S. C. C. & SMITS, A. J. 2013 Turbulence spectra in smooth- and rough-wall pipe flow at extreme Reynolds numbers. *J. Fluid Mech.* **731**, 46–63.

SADDOUGHI, S. G. & VEERAVALLI, S. V. 1994 Local isotropy in turbulent boundary layers at high Reynolds number. *J. Fluid Mech.* **268**, 333–372.

SEGALINI, A., ÖRLÜ, R., SCHLATTER, P., ALFREDSSON, P. H., RÜEDI, J.-D. & TALAMELLI, A. 2011 A method to estimate turbulence intensity and transverse Taylor microscale in turbulent flows from spatially averaged hot-wire data. *Exp. Fluids* **51** (3), 693.

SILLERO, J. A., JIMÉNEZ, J. & MOSER, R. D. 2013 One-point statistics for turbulent wall-bounded flows at Reynolds numbers up to $\delta^+ \approx 2000$. *Phys. Fluids* **25** (10), 105102.

SMITS, A. J., MONTY, J. P., HULTMARK, M., BAILEY, S. C. C., HUTCHINS, N. & MARUSIC, I. 2011 Spatial resolution correction for wall-bounded turbulence measurements. *J. Fluid Mech.* **676**, 41–53.

SREENIVASAN, K. R. 1995 On the universality of the Kolmogorov constant. *Phys. Fluids* **7** (11), 2778–2784.

TALAMELLI, A., PERSIANI, F., FRANSSON, J. H. M., ALFREDSSON, P. H., JOHANSSON, A. V., NAGIB, H. M., RÜEDI, J.-D., SREENIVASAN, K. R. & MONKEWITZ, P. A. 2009 CICLoPE: a response to the need for high Reynolds number experiments. *Fluid Dyn. Res.* **41** (2), 021407.

TALAMELLI, A., SEGALINI, A., ÖRLÜ, R., SCHLATTER, P. & ALFREDSSON, P. H. 2013 Correcting hot-wire spatial resolution effects in third- and fourth-order velocity moments in wall-bounded turbulence. *Exp. Fluids* **54** (4), 1496.

TALLURU, K. M., KULANDAIVELU, V., HUTCHINS, N. & MARUSIC, I. 2014 A calibration technique to correct sensor drift issues in hot-wire anemometry. *Meas. Sci. Technol.* **25** (10), 105304.

TAYLOR, G. I. 1938 The spectrum of turbulence. *Proc. R. Soc.* A **164**, 476–490.

TOWNSEND, A. A. 1976 *The Structure of Turbulent Shear Flow*. Cambridge University Press.

VALLIKIVI, M., GANAPATHISUBRAMANI, B. & SMITS, A. J. 2015*a* Spectral scaling in boundary layers and pipes at very high Reynolds numbers. *J. Fluid Mech.* **771**, 303–326.

VALLIKIVI, M., HULTMARK, M. & SMITS, A. J. 2015*b* Turbulent boundary layer statistics at very high Reynolds number. *J. Fluid Mech.* **779**, 371–389.

VALLIKIVI, M. & SMITS, A. J. 2014 Fabrication and characterization of a novel nanoscale thermal anemometry probe. *J. Microelectromech. Syst.* **23** (4), 899–907.

VINCENTI, P., KLEWICKI, J., MORRILL-WINTER, C., WHITE, C. M. & WOSNIK, M. 2013 Streamwise velocity statistics in turbulent boundary layers that spatially develop to high Reynolds number. *Exp. Fluids* **54** (12), 1–13.

WILLERT, C. E., SORIA, J., STANISLAS, M., KLINNER, J., AMILI, O., EISFELDER, M., CUVIER, C., BELLANI, G., FIORINI, T. & TALAMELLI, A. 2017 Near-wall statistics of a turbulent pipe flow at shear Reynolds numbers up to 40 000. *J. Fluid Mech.* **826**, R5.